DOI 10.24425/aee.2024.148868

Voltage regulation strategy for alternating current microgrid under false data injection attacks

Rongqiang Guan [1]✉, Jing Yu [1], Siyuan Fan [2], Tianyi Sun [2] Peng Liu [2], Han Gao [2]

[1] *Jilin Engineering Normal University, Changchun, 130000, China*

[2] *Northeast Electric Power University, Jilin, 132000, China*

e-mail: guanrq@jlenu.edu.cn, yujing@jlenu.edu.cn, fans@neepu.edu.cn, sty313@neepu.edu.cn, 20202962@neepu.edu.cn, 13844609588@163.com

(Received: 08.08.2023, revised: 01.03.2024)

Abstract: This study introduces a robust strategy for regulating output voltage in the presence of false data injection (FDI) attacks. Employing a hierarchical approach, we disentangle the distributed secondary control problem into two distinct facets: an observer-based resilient tracking control problem and a decentralized control problem tailored for real systems. Notably, our strategy eliminates the reliance on global information and effectively mitigates the impact of FDI attacks on directed communication networks. Ultimately, simulation results corroborate the efficacy of our approach, demonstrating successful voltage regulation within the system and proficient management of FDI attacks.

Key words: communication link faults, directed graph, FDI attacks, fully distributed control, voltage regulation control

1. Introduction

A microgrid (MG) represents a compact power system integrating distributed energy sources, loads, and energy storage devices, utilizing alternating current for energy transmission and distribution [1]. The control architecture of an MG comprises three levels: primary control, secondary control, and tertiary control. Primary control focuses on the operational aspects of MG equipment, including voltage stabilization. In contrast, secondary control assumes a higher-level role, primarily dedicated to voltage restoration and maintenance within the MG. Tertiary control operates at the highest level, overseeing the overall coordination, energy distribution management, optimization, and external interactions within the MG [2].

© 2024. The Author(s). This is an open-access article distributed under the terms of the Creative Commons Attribution-NonCommercial-NoDerivatives License (CC BY-NC-ND 4.0, https://creativecommons.org/licenses/by-nc-nd/4.0/), which permits use, distribution, and reproduction in any medium, provided that the Article is properly cited, the use is non-commercial, and no modifications or adaptations are made.

This paper addresses the challenge of secondary voltage regulation in MGs. Secondary controls are traditionally categorized as decentralized control, centralized control, and distributed control [3]. Distributed control employs communication between neighboring distributed generators (DGs) to achieve consensus through mutual information exchange [4–6]. In this approach, each DG collaborates with its neighboring units, facilitating joint decision-making and coordinated actions. Distributed control circumvents the limitations of centralized control, such as a single point of failure, while retaining some advantages of decentralized control, such as local autonomy and rapid response. A noteworthy trend in MG control is the growing prevalence of distributed control as the predominant approach for secondary control in MGs [7–9].

In recent years, researchers have advanced diverse distributed control methods tailored to address specific challenges encountered in MG operations. Notably, the work presented in [10] introduces a distributed consensus protocol designed to address issues related to accurate reactive, harmonic, and unbalanced power sharing within MGs. This protocol ensures that DGs within the MG converge to a consensus on power sharing, thereby enhancing the overall system performance. The approach presented in [11] proposes a consensus-based distributed finite-time regulator to coordinate the active power, frequency and output voltage of an islanded MG. This methodology facilitates effective coordination and control among DGs, even in islanded operational scenarios. Additionally, the study outlined in [12] concentrates on distributed secondary control for isolated AC MGs in the presence of external disturbances. It is crucial to acknowledge that while these distributed secondary control strategies [8–12] exhibit promising outcomes, they often presume ideal conditions where the communication network is fully known. However, in the real-world scenario of a MG system, the global information and topology of the communication network may be unknown [13]. Therefore, a critical consideration is how to achieve a fully distributed control approach under an unknown communication network, relying solely on information from neighboring DGs.

Moreover, in practical scenarios, the susceptibility of electrical components in MGs to failures resulting from attacks has been well-documented [14, 15]. In response to this challenge, diverse resilient control schemes have been proposed, aiming to ensure stable voltage and frequency regulation within closed-loop systems [16, 17]. Notably, existing resilient control strategies for MGs often assume ideal communication links [17, 18], disregarding the real-world complexities introduced by physical variations, external noise, and potential channel manipulation by hostile nodes [19, 20]. The pursuit of high reliability in MGs necessitates resilient control mechanisms capable of addressing communication failures. Several distributed control schemes have emerged to tackle this aspect, encompassing strategies for frequency/voltage restoration and proportional power sharing that explicitly account for communication delays [21]. Previous work successfully demonstrated the recovery of output voltage and frequency of a DG inverter subject to additive noise using a resilient control approach [22]. However, the specific challenge of communication link failures caused by FDI attacks during output voltage regulation of AC MGs remains an open issue that needs to be fully investigated. Advancements in this domain are imperative for enhancing the resilience and reliability of AC MG operations.

In light of the aforementioned constraints, this paper introduces a novel secondary voltage resilience regulation strategy tailored to AC MGs in the presence of FDI attacks. The primary objective is to enhance the resilience and adaptability of MGs when confronted with challenging operating conditions.

Distinguishing itself from existing literature [8, 9, 11–13, 16, 17, 21–23], our study uniquely addresses the intricacies of regulating the output voltage of distributed power supply in scenarios involving communication network failures under FDI attacks. The resilient control strategy presented herein is fully distributed and circumvents the limitations associated with global information and fault parameters of the communication network by leveraging adaptive techniques.

Unlike traditional secondary control strategies based on undirected graph communication [8, 11–13, 16, 17, 21–23], our strategy is adapted to directed communication networks such that its Laplace matrix is asymmetric. This property complicates the design of resilient control strategies.

The paper is structured as follows:

In Section 2, the modeling framework and the corresponding resilient control method used to solve the AC MG output regulation problem are presented. Section 3 is dedicated to the validation and verification of the proposed control method. In Section 4, we summarize the key findings and contributions of this paper.

2. Methods

In this study, we focus on the regulation problem of output voltages in an MG comprising N DGs. The dynamic model of each DG is comprehensive, encompassing various components such as droop control, inner-loop voltage and current control, LC filter, containment-based voltage secondary control, and the line model. This model is depicted in Fig. 1.

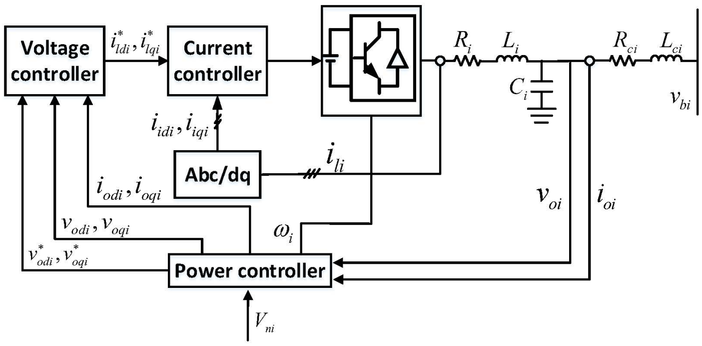

Fig. 1. Block diagram of an inverter-based DG

The nonlinear dynamic model of the AC MG in a compact form is

$$\begin{aligned} \dot{o}_i &= f_i(o_i) + k_i(o_i) J_i + g_i(o_i) u_i, \\ y_i &= d_i(o_i), \end{aligned} \tag{1}$$

where the state vector is

$$o_i = [\delta_i, P_i, Q_i, \phi_{v_{di}}, \phi_{v_{qi}}, \phi_{i_{di}}, \phi_{i_{qi}}, i_{ldi}, i_{lqi}, v_{odi}, v_{oqi}, i_{odi}, i_{oqi}]^T \tag{2}$$

and

$$J_i = [\omega_{\text{com}}, v_{bdi}, v_{bqi}].$$

Detailed expressions for o_i, $f_i(o_i)$, $g_i(o_i)$, and $k_i(o_i)$ can be extracted from [9]. Moreover, y_i is set to v_{odi}. u_i is the virtual controller to be designed in this paper.

Then, by feedback linearization, we have

$$\ddot{y}_i = L_{F_i}^2 d_i + L_{g_i} L_{F_i} d_i V_{ni} = u_i, \tag{3}$$

where: $F_i = f_i(o_i) + k_i(o_i)J_i$, $L_{F_i} d_i = \dfrac{\partial d_i}{\partial x_i} F_i$ and $L_{F_i}^2 d_i = L_{F_i}(L_{F_i} d_i) = \dfrac{\partial L_{F_i} d_i}{\partial x_i} F_i$ are the Lie derivatives of d_i along F_i.

The control input V_{ni} is implemented by u_i as

$$V_{ni} = (L_{g_i} L_{F_i} d_i)^{-1}(-L_{F_i}^2 d_i + u_i). \tag{4}$$

Then,

$$\begin{aligned} \dot{z}_{vi}(t) &= A z_{vi}(t) + B u_i, \\ y_i(t) &= C z_{vi}(t), \end{aligned} \tag{5}$$

where: $z_{vi} = [v_{odi}, \dot{v}_{odi}]^T$, $A = \begin{bmatrix} 0 & 1 \\ 0 & 0 \end{bmatrix}$, $B = \begin{bmatrix} 0 \\ 1 \end{bmatrix}$, $C = [1, 0]$.

The dynamic of reference virtual leader is shown as follows:

$$\dot{z}_{v0}(t) = A z_{v0}(t), \tag{6}$$

where $z_{v0} = [v_{\text{ref}}, \dot{v}_{\text{ref}}]^T$, and v_{ref} represents the reference voltage regulation.

2.1. Problem statement

The communication structure among the N DGs in the MG can be represented by a graph $G(C, T)$, where $C = \{c_1, c_2, \ldots, c_N\}$ denotes the set of nodes, and $T \subseteq C \times C$ represents the set of edges. The weighted adjacency matrix $D = [b_{ij}] \in \mathbf{Rn}^{(N+1)\times(N+1)}$ is defined such that $b_{ij} = 1$ if there exists a communication link between nodes c_i and c_j (i.e., $(c_i, c_j) \in T$, and $b_{ij} = 0$ otherwise).

To characterize the graph structure, the nonsymmetric Laplacian matrix $L = [L_{ij}]$ is introduced, where L_{ii} is the sum of weights associated with node c_i, and L_{ij} is the negative weight between nodes c_i and c_j for $i \neq j$.

Assumption 1 The communication topology between the DGs is directed, indicating that the information flow has specified directions among the nodes. Additionally, the dynamics of the virtual leader are directed towards all DGs.

Assumption 1 represents the fundamental standard assumption for consensus control in MASs.

2.2. Attack model and analysis

The coupling between the information system and the physical system in the distributed control strategy makes the MG CPS architecture more vulnerable to cyber attacks. An attacker can inject malicious measurement data into the secondary controller and attack the communication links of the power system, thereby destabilizing and disrupting the operation of the power grid. In this paper, we define $\mathbf{Rn}^{(n\times m)}$ to be an $n \times m$ dimensional real number field.

The communication links faults under FDI attack:

$$b_{ij}^{f}(t) = b_{ij} + \delta_{ij}^{b}(t), \quad i = 1, 2, \ldots, N, \quad j = 0, 1, \ldots, N, \tag{7}$$

where $\delta_{ij}^{b}(t)$ represents the corrupted weight resulting from communication faults. As a consequence of this fault model, the communication link weights become time-varying and unknown due to the presence of $\delta_{ij}^{b}(t)$. The uncertainty introduced by these corrupted weights poses a challenge in effectively estimating and controlling the communication dynamics among the DGs.

Assumption 2 The communication link faults $\delta_{ij}^{b}(t)$, where $i = 1, 2, \ldots, N$ and $j = 0, 1, \ldots, N$, as well as their derivatives, are bounded but remain unknown. Additionally, the signs of b_{ij}^{f} are consistent with those of b_{ij}.

Due to the communication link faults (7), the Laplace matrix is redefined as $L^{f}(t) = J(t) - D(t)$, where $D(t) = [b_{ij}^{f}(t)]$ is the adjacency matrix and $J(t) = \operatorname{diag}\left\{\sum_{j \in N_i} b_{ij}^{f}(t)\right\}$ is the in-degree matrix.

Then, $L^{f}(t)$ is defined as

$$L^{f}(t) = \begin{bmatrix} 0_{1\times 1} & 0_{1\times N} \\ L_2^{f}(t) & L_1^{f}(t) \end{bmatrix}. \tag{8}$$

The matrices $L_2^{f}(t) \in \mathbf{Rn}^{(N+1)}$ and $L_1^{f}(t) \in \mathbf{Rn}^{(N\times N)}$ are defined, where $L_1^{f}(t)$ has eigenvalues with positive real parts. It can be readily demonstrated that $L_1^{f}(t)$ is a nonsingular M-matrix.

Lemma 1 [22] Under the assumption that both Assumption 1 and Assumption 2 hold, it follows that there exists a positive infinite diagonal matrix $K(t)$ satisfying the equation $K(t)L_1^{f}(t) + \left(L_1^{f}(t)\right)^{T} K(t) = N(t)$, where $N(t)$ is positive. Consequently, both $K(t)$ and $\dot{K}(t)$ are bounded.

The dynamic model of the i-th DG is

$$[b] \begin{aligned} \dot{x}_i(t) &= A z_{vi}(t) + B u_i, \\ y_{vi}(t) &= C z_{vi}(t). \end{aligned} \tag{9}$$

2.3. Main result

The objective of this section is to achieve co-regulation of the output voltages v_{odi}, $i = 1, 2, \ldots, N$, within an MG. To achieve this, we develop a secondary voltage strategy that considers the communication links.

The state observer $\hat{x}_i$ to estimates $z_{vi} i = 1, 2, \ldots, N$ is as follows:

$$[b] \begin{aligned} \dot{\hat{x}}_i(t) &= A\hat{x}_i(t) + \hat{u}_i, \\ \hat{y}_i(t) &= C\hat{x}_i(t), \end{aligned} \tag{10}$$

where $\hat{x}_i(t)$, $\hat{y}_i(t)$ are the estimations of $z_{vi}(t)$, $y_{vi}(t)$, respectively. $L \in \mathbf{Rn}^{2\times 1}$ is the observer gain.

Let the observer controller $\hat{u}_i$ in (10) be

$$\hat{u}_i = -c(\iota_i + \psi_i) Q_v \upsilon_i(t), \tag{11}$$

where

$$\dot{\iota}_i = -\nu_{\iota_i}(\iota_i - 1) + \upsilon_i^T(t)Q_v Q_v \upsilon_i(t), \tag{12}$$

$$\psi_i = \upsilon_i^T(t)Q_v \upsilon_i(t), \tag{13}$$

where c, ν_{ι_i} are positive constants. Moreover, $\upsilon_i = \sum_{j=0}^{N} b_{ij}^f(\hat{x}_i(t) - \hat{x}_j(t))$. Moreover, $\iota_i(0) \geq 1$. Then, $\iota_i(t) \geq 1$ for any $t > 0$.

Define $\eth = \text{col}\{\eth_1(t), \eth_2(t), \ldots, \eth_N(t)\}$, then

$$\eth_i = \hat{x}_i - x_{\text{ref}}, \tag{14}$$

where $\hat{x} = \text{col}\{\hat{x}_1(t), \hat{x}_2(t), \ldots, \hat{x}_N(t)\}$.

Then,

$$\upsilon = \left(L_1^f(t) \otimes I_2\right)\eth, \tag{15}$$

where $\upsilon = \text{col}\{\upsilon_1(t), \upsilon_2(t), \ldots, \upsilon_N(t)\}$.

Then,

$$\dot{\hat{x}}_i(t) = A\hat{x}_i(t) - c(\iota_i + \psi_i)Q_v \upsilon_i(t) - LC\alpha_i, \tag{16}$$

where $\alpha_i = \hat{x}_i - z_{vi}$.

Due to $\upsilon = \left(L_1^f(t) \otimes I_2\right)\eth$, we obtain the dynamics of υ as follows:

$$\dot{\upsilon} = (L_1(t) \otimes I_2)\,\eth + (I_N \otimes A)\,\upsilon - [cL_1(t)(\iota + \psi) \otimes Q_v]\upsilon - (L(t) \otimes LC)\,\alpha, \tag{17}$$

where $\iota = \text{diag}\{\iota_1, \iota_2, \ldots, \iota_N\}$, $\psi = \text{diag}\{\psi_1, \psi_2, \ldots, \psi_N\}$, $\alpha = \text{col}\{\alpha_1, \alpha_2, \ldots, \alpha_N\}$.

The u_i in (5) be

$$u_i = -c(\iota_i + \psi_i)B^T Q_v \upsilon_i(t). \tag{18}$$

Then:

$$\dot{\alpha}_i = (A - LC)\,\alpha_i + c\left(I_2 - BB^T\right)(\iota_i + \psi_i)\,Q_v \upsilon_i(t). \tag{19}$$

It shows that

$$\dot{\alpha} = \mathcal{A}\alpha + \left[c(\iota + \psi) \otimes \left(I_2 - BB^T\right)Q_v\right]\upsilon, \tag{20}$$

where $\mathcal{A} = I_N \otimes (A - LC)$.

Theorem 1 Suppose Assumptions 1, 2, 3 hold, and there exist appropriate $\pi_1 > 0$, $Q_v > 0$, $\Gamma > 0$, $V > 0$, L are with appropriate dimensions such that

$$Q_v A^T + AQ_v - Q_v Q_v + \eta I_2 = 0, \tag{21}$$

$$\Gamma\mathcal{A} + \mathcal{A}^T\Gamma + \pi_1^{-1}c\Gamma\Gamma + \pi_3^{-1}\left(I_N \otimes C^T L^T LC\right) = -V. \tag{22}$$

Subsequently, the consensus error vector will exhibit exponential convergence towards a bounded domain. Consider the following Lyapunov function candidate

$$V = V_1 + V_2, \tag{23}$$

where

$$V_1 = \alpha^T \Gamma \alpha, \tag{24}$$

$$V_2 = \frac{1}{2}\sum_{i=1}^{N} k_i \left(2\iota_i + \psi_i\right)\psi_i + \frac{1}{2}\sum_{i=1}^{N} s_i \left(\iota_i - \iota_{Ai}\right)^2, \tag{25}$$

s_i and ι_{Ai} represent positive constants.

Then, we obtain that

$$\dot{V}_1 = 2\alpha^T \Gamma \dot{\alpha} = 2\alpha^T \Gamma A \alpha + 2\alpha^T \Gamma \left[c\left(\iota + \psi\right) \otimes \left(I_2 - BB^T\right) Q_v\right] \upsilon. \tag{26}$$

Applying Young's inequality, with π_1 being a positive constant, we can deduce the following expression:

$$\begin{aligned} &2\alpha^T \Gamma \left[c\left(\iota + \psi\right) \otimes \left(I_2 - BB^T\right) Q_v\right] \upsilon \\ &\quad \leq \pi_1^{-1} c \alpha^T \Gamma \Gamma \alpha + \pi_1 \|I_2 - BB^T\|^2 c \sum_{i=1}^{N} (\iota_i + \psi_i)^2 \upsilon_i^T Q_v Q_v \upsilon_i. \end{aligned} \tag{27}$$

Then,

$$2\alpha^T \Gamma \dot{\alpha} \leq 2\alpha^T \Gamma A \alpha + \pi_1^{-1} c \alpha^T \Gamma \Gamma \alpha + \pi_1 c \|I_2 - BB^T\|^2 \sum_{i=1}^{N} (\iota_i + \psi_i)^2 \upsilon_i^T Q_v Q_v \upsilon_i. \tag{28}$$

Subsequently, by taking the derivative of V_2, utilizing Eqs. (12) and (13), we obtain the following result:

$$\dot{V}_2 = \sum_{i=1}^{N} k_i \left(\iota_i + \psi_i\right) \dot{\psi}_i + \sum_{i=1}^{N} k_i \dot{\iota}_i \psi_i + \sum_{i=1}^{N} s_i \left(\iota_i - \iota_{Ai}\right) \dot{\iota}_i + \frac{1}{2}\sum_{i=1}^{N} \dot{k}_i \left(2\iota_i + \psi_i\right) \psi_i. \tag{29}$$

Then,

$$\begin{aligned} \dot{V}_2 = \sum_{i=1}^{N} k_i \left(\iota_i + \psi_i\right) \dot{\psi}_i = \upsilon^T &\left[\left(\iota + \psi\right) K\left(t\right)_1 \left(t\right) \otimes Q_v\right] \dot{o} \\ &+ \upsilon^T \left[\left(\iota + \psi\right) K\left(t\right) \otimes \left(Q_v A + A^T Q_v\right)\right] \upsilon \\ &- 2c\upsilon^T \left[\left(\iota + \psi\right) K\left(t\right) L_1\left(t\right) \left(\iota + \psi\right) \otimes Q_v BB^T Q_v\right] \upsilon \\ &- 2\upsilon^T \left[\left(\iota + \psi\right) K\left(t\right) L_1\left(t\right) \otimes Q_v LC\right] \alpha. \end{aligned} \tag{30}$$

By utilizing Eqs. (14) and (15), we can deduce that $\|\dot{o}\| \leq \|(L_1^f)^{-1}(t)\| \, \|\upsilon\|$. Let K_m denote the lower bound of $K(t)$. For any positive constant π_2, the following result can be derived:

$$\begin{aligned} 2\upsilon^T \left[(\iota + \psi)_1(t) \otimes Q_v\right] \dot{o} \leq{} & \frac{\pi_2}{K_m \lambda_{\min}(Q_v)} \upsilon^T [(\iota + \psi) K(t) \otimes Q_v Q_v] \upsilon \\ &+ \frac{\lambda_{\max}\left(\dot{L}_1^T(t) \dot{L}_1(t)\right) \|(L_1^f(t))^{-1}\|^2}{\pi_2 K_m \lambda_{\min}(Q_v)} \upsilon^T \left[(\iota + \psi) K(t) \otimes Q_v Q_v\right] \upsilon. \end{aligned} \tag{31}$$

Applying Lemma 1, where the minimum eigenvalue of $N(t)$ is denoted by λ_0, we can deduce the following conclusion:

$$\begin{aligned}
-2c\upsilon^T\left[(\iota+\psi)K(t)L_1(t)(\iota+\psi)\otimes Q_vQ_v\right]\upsilon = \\
&-c\upsilon^T[(\iota+\psi)(K(t)L_1(t)+L_1^T(t)K(t))(\iota+\psi)\otimes Q_vQ_v]\upsilon \\
&\le -c\lambda_0\sum_{i=1}^{N}(\iota_i+\psi_i)^2\upsilon_i^TQ_vQ_v\upsilon_i\,.
\end{aligned} \tag{32}$$

Let us define the maximum eigenvalue of $K(t)L_1(t)L_1^T(t)K(t)$ as λ_Ξ. For any positive constants π_3 and π_4, it can be readily deduced that:

$$\begin{aligned}
-2\upsilon^T\left[(\iota+\psi)K(t)L_1(t)\otimes Q_vLC\right]\alpha \le \\
&\pi_3\sum_{i=1}^{N}\lambda_\Xi\left(\iota_i+\psi_i\right)^2\upsilon_i^TQ_vQ_v\upsilon_i+\pi_3^{-1}\sum_{i=1}^{N}\alpha_i^TC^TL^TLC\alpha_i.
\end{aligned} \tag{33}$$

By choosing $s_i>0$ to be sufficiently large such that $s_i\geqslant\max_{i=1,2,\dots,N}k_i$,

$$\begin{aligned}
\sum_{i=1}^{N}k_i\dot{\iota}_i\psi_i+\sum_{i=1}^{N}s_i\left(\iota_i-\iota_{Ai}\right)\dot{\iota}_i &= \upsilon^T\left[\psi K(t)\otimes Q_vQ_v\right]\upsilon-\sum_{i=1}^{N}k_i\nu_{\iota i}\psi_i(\iota_i-1) \\
&+\upsilon^T\left[s(\iota-\bar{\iota})\otimes Q_vQ_v\right]\upsilon-\sum_{i=1}^{N}s_i\nu_{\iota i}(\iota_i-\iota_{Ai})(\iota_i-1) \\
&\le\upsilon^T\left[s(\psi+\iota-\bar{\iota})K(t)\otimes Q_vQ_v\right]\upsilon-\sum_{i=1}^{N}k_i\nu_{\iota i}(\iota_i+\psi_i-\iota_{Ai})(\iota_i-1).
\end{aligned} \tag{34}$$

Let $\dot{k}_M$ be defined as the upper bound of (t). Then, we have the following result:

$$\frac{1}{2}\sum_{i=1}^{N}\dot{k}_i(2\iota_i+\psi_i)\psi_i\le\frac{\dot{K}_M}{K_m\lambda_{\min}\left(Q_v\right)}\upsilon^T\left[K(t)(\iota+\psi)\otimes Q_vQ_v\right]\upsilon. \tag{35}$$

It can be deduced from (28–35) that (29) satisfies the following condition:

$$\begin{aligned}
\dot{V}=\dot{V}_1+\dot{V}_2 &\le 2\alpha^T\Gamma A\alpha+\pi_1^{-1}c\alpha^T\Gamma\Gamma\alpha+\pi_3^{-1}\sum_{i=1}^{N}\alpha_i^TC^TL^TLC\alpha_i \\
&+\upsilon^T(\iota+\psi)K(t)\otimes\left\{Q_vA+A^TQ_v+\varsigma Q_vQ_v\right\}\upsilon \\
&-\sum_{i=1}^{N}\left\{[c\lambda_0-(\pi_3+\pi_4)\lambda_\Xi-\pi_1c\|I_2-BB^T\|^2](\iota_i+\psi_i)^2+s_i\iota_{Ai}k_i\right\}\|Q_v\upsilon_i\|^2 \\
&+\sum_{i=1}^{N}\frac{\nu_{\iota_i}k_i}{4}(\iota_i-1)^2-\sum_{i=1}^{N}k_i\nu_{\iota_i}(\iota_i+\psi_i-\iota_{Ai})(\iota_i-1),
\end{aligned} \tag{36}$$

where

$$\varsigma=s_i+\frac{\pi_2+\pi_2^{-1}\lambda_{\max}(\dot{L}_1^T(t)\dot{L}_1(t))\|(L_1^f(t))^{-1}\|^2+\dot{K}_M}{K_m\lambda_{\min}(Q_v)}.$$

Sufficiently small π_1, π_3, π_4 such that $\widetilde{n} = c\lambda_0 - (\pi_3 + \pi_4)\lambda_\Xi - \pi_1 c\|I_2 - BB^T\|^2 > 0$ hold. $\grave{o}_i$ is a positive constant. Moreover, a sufficiently large $\iota_{Ai} > 0$ can ensure that $\iota_{Ai} > \max\left\{\frac{1+\varsigma+s_i^2K_m^2}{4\widetilde{n}s_ik_i}, \frac{1}{\beta_ik_i\varpi_2}, \frac{1}{\beta_i}, \frac{1}{\beta_ik_i\varpi_1}, \frac{W_{2i}}{\beta_i}, \frac{W_{2i}}{\beta_i}\right\}$ holds.

Note that

$$-(\iota_i - 1)(\iota_i - \iota_{Ai}) = -(\iota_i - \iota_{Ai})^2 - (\iota_{Ai} - 1)(\iota_i - \iota_{Ai}) \leq -\frac{1}{2}(\iota_i - \iota_{Ai})^2 + \frac{1}{2}(\iota_{Ai} - 1)^2 \tag{37}$$

and

$$-(\iota_i - 1)(\iota_i - \iota_{Ai}) = -(\iota_i - 1)^2 - (\iota_{Ai} - 1)(\iota_i - \iota_{Ai}) \leq -\frac{1}{2}(\iota_i - 1)^2 + \frac{1}{2}(\iota_{Ai} - 1)^2. \tag{38}$$

Furthermore

$$-\sum_{i=1}^{N} k_i\nu_{\iota_i}(\iota_i - \iota_{Ai})(\iota_i - 1) = \sum_{i=1}^{N} \frac{k_i\nu_{\iota_i}}{2}(\iota_{Ai} - 1)^2 - \frac{k_i\nu_{\iota_i}}{4}[(\iota_i - \iota_{Ai})^2 + (\iota_i - 1)^2]. \tag{39}$$

Then,

$$\begin{aligned}\dot{V} \leq & -\delta V - \upsilon^T((\iota + \psi)K(t) \otimes (I_N - \delta Q_v)\upsilon - \alpha^T(V - \delta\Gamma)\alpha \\ & - \sum_{i=1}^{N}\left(\frac{\nu_{\iota_i}k_i}{4} - \frac{\delta s_i}{2}\right)(\iota_i - \iota_{Ai})^2 + \frac{1}{2}\sum_{i=1}^{N} k_i\nu_{\iota_i}(\iota_{Ai} - 1)^2.\end{aligned} \tag{40}$$

Moreover, based on the condition

$$0 < \delta \leq \min_{i=1,2,\ldots,N}\left\{\frac{\nu_{\iota_i}k_i}{2s_i}\frac{1}{2\lambda_{\max}(Q_v)}\frac{1}{2\lambda_{\max}(\Gamma)}, 2\grave{o}_i\Gamma_{W_i}\right\},$$

(36) satisfies the following inequality:

$$\dot{V} \leq -\delta V + \Xi. \tag{41}$$

Therefore α, ι and υ can converge exponentially to the following bounded set:

$$D \triangleq \left\{\alpha, \upsilon, \iota : V \leq \frac{1}{\delta}\Xi\right\}. \tag{42}$$

Therefore, the algorithm designed in this chapter can be able to achieve a reasonable regulation of the output voltage under the FDI attack to restore the voltage to the reference value.

3. Results and discussion

This section is dedicated to validating the practicality and effectiveness of the proposed approach in responding to FDI attacks. Simulations were conducted within the MATLAB/Simulink software environment, utilizing a MG configuration depicted in Fig. 2. The MG consists of four DGs, and the specific parameters are outlined in Table 1. The communication topology among DGs is illustrated in Fig. 2. Specifically, DG#1 received information from v_{ref}.

To simulate a real-world scenario, the proposed resilient voltage regulation approach was applied to the MG during islanding, commencing at $t = 0.0$ s. The simulation unfolds as follows:

1. Initialization ($t = 0.0$ s): The proposed resilient voltage regulation approach is initiated.
2. Voltage regulation ($t = 0.5$ s): The output voltage regulation secondary control takes effect.
3. Load adjustment ($t = 1.0$ s): Load #1 is reduced by 50%.
4. Load restoration ($t = 1.5$ s): 50% of Load #1 is restored to its original value.

Table 1. Simulation system parameters

DGs	$m_P = 1.5 \times 10^{-5}, \quad n_Q = 2 \times 10^{-4}$
Lines	$R_{l1} = R_{l3} = 1e - 4\ \Omega, \quad R_{l2} = 1e - 4\ \Omega$
	$L_{l1} = L_{l3} = 3.18e - 4$ mH, $\quad L_{l2} = 1.847$ mH
RL loads	$P = 100$ kW, $\quad Q = 120$ kvar

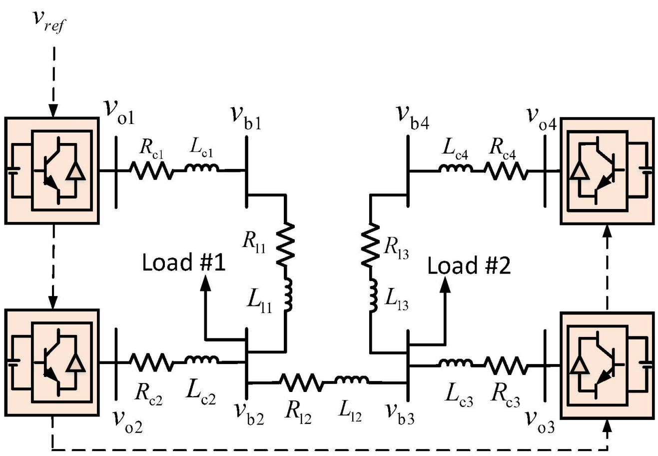

Fig. 2. The example MG test system

We define $v_{\mathrm{ref}} = 220$. The attack vector of the FDI attack is simulated as $a_{ij}^{f} = 0.1 * i \sin(t + 0.1 * j)$. The parameters of the output voltage algorithm are chosen as $c = 1.5e + 7$, $\nu_{\iota_i} = 1$, $\iota_{y_{v i}} = 5$, $\iota_i(0.4) = 1$.

Solving (24) gives a solution

$$Q_v = \begin{bmatrix} 0.9102 & 0.4142 \\ 0.4142 & 1.2872 \end{bmatrix}$$

These scenarios were carefully chosen to comprehensively evaluate the system's response under different conditions. The directed communication topology ensures that DGs exchange information effectively.

These scenarios were carefully chosen to comprehensively evaluate the system's response under different conditions. The directed communication topology ensures that DGs exchange information effectively. The proposed simulation scenarios provide a nuanced understanding of how the proposed approach adapts to various variations, demonstrating its robustness in terms of load transformation.

The efficacy of the output voltage regulation algorithm in the MG is systematically validated through a series of diverse test scenarios. Initially, the algorithm employs primary control, dynamically adjusting the drop factor to sustain voltage stability, as vividly illustrated in Fig. 3. This primary control mechanism aptly achieves voltage stability and exhibits a prompt response. The primary control successfully achieves voltage stability and responds promptly. Upon activation of the secondary control algorithm at $t = 0.5$ s, the output voltages are regulated to reference values v_{ref}. At $t = 1$ s and $t = 1.5$ s, the proposed output voltage regulation strategy effectively restores the desired voltage level after temporary load disconnection and reconnection. Figures 4–6 complementarily depict the corresponding changes in active power, reactive power, and bus voltages, further accentuating the effectiveness of the proposed voltage regulation approach.

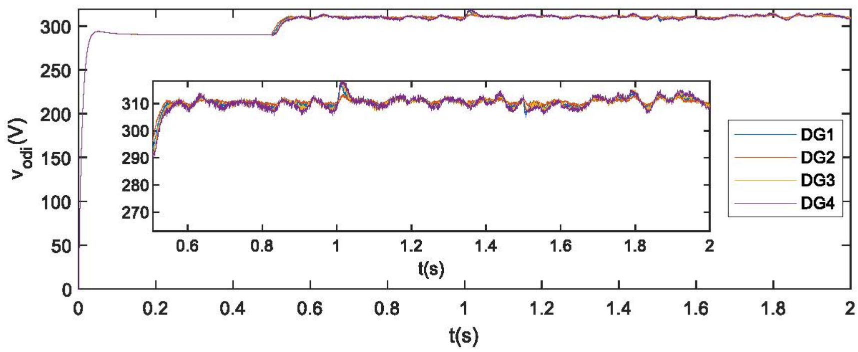

Fig. 3. Output terminal voltage v_{odi}, $i = 1, 2, \ldots, 4$

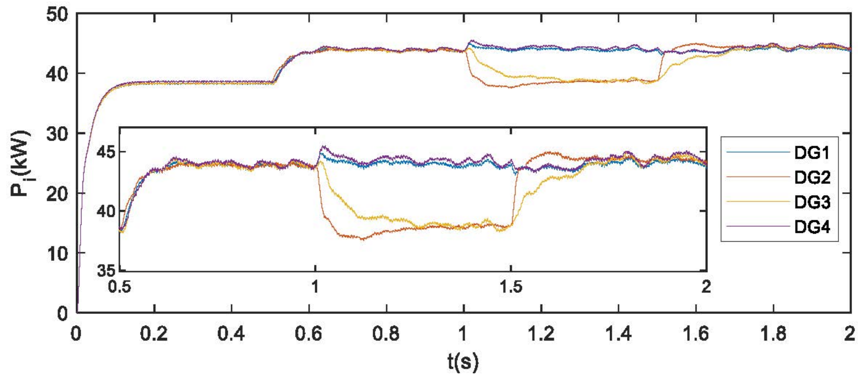

Fig. 4. The active power P_i, $i = 1, 2, \ldots, 4$

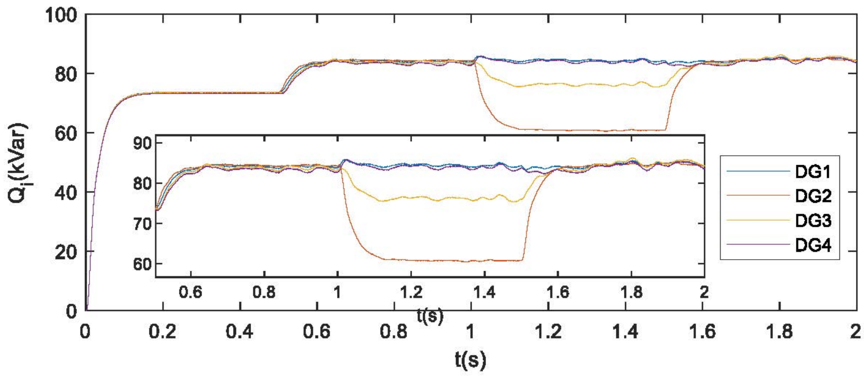

Fig. 5. The reactive power Q_i, $i = 1, 2, \ldots, 4$

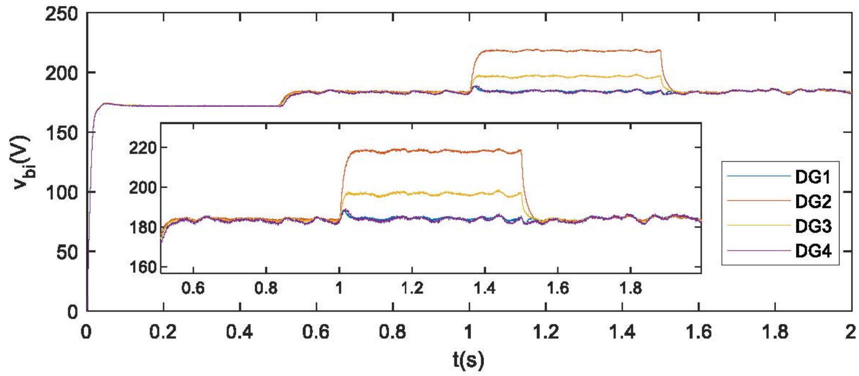

Fig. 6. The bus voltages v_{bdi}, $i = 1, 2, \ldots, 4$

In summary, the proposed strategy stands verified for its effectiveness under load shifting and plugging scenarios, thereby offering a robust and reliable means to ensure the stable operation of the MG. This validation reinforces the viability and practicality of the proposed approach in real-world scenarios.

4. Conclusions

This paper presents a secondary control strategy designed to regulate the output voltage of a robust AC MG under the influence of FDI attacks. In response to these challenges, this paper introduces a resilient fault-tolerant control algorithm grounded in state observer output feedback. This innovative approach is geared toward enhancing communication resilience, with the added advantage of negating the requirement for comprehensive global information about the directed communication network and reducing dependence on application-specific fault parameters. The proposed strategy not only demonstrates resilience but also excels in handling practical constraints. By addressing communication challenges and minimizing dependencies on intricate parameters, this paper's approach emerges as an efficient and practical solution.

Nomenclature

$I_N \in \mathbf{Rn}^{(N\times N)}$	is the identity matrix
$\lambda_{\max}(*)$	is the maximum eigenvalue of matrix $*$
$\|\cdot\|$	is the Euclidean norm of a vector
$\operatorname{diag}\{a_1,\ldots,a_N\}$	is the diagonal matrix with elements $a_1, a_2, \ldots, a_N$ on main diagonal
$\operatorname{col}\{a_1,a_2,\ldots,a_N\}$	is the column vector formed by stacking elements $a_1, a_2, \ldots, a_N$ vertically
$\otimes$	is the Kronecker product of matrices

Acknowledgements

This work was supported by Science and Technology Development Plan Project of Jilin Province, Grant No. 20210203048SF.

References

[1] Zhang Z., Zhang B., Wang D. *et al.*, *Battery/super-capacitor HESS applied in DC microgrid*, Archives of Electrical Engineering,vol. 69, no. 2, pp. 379–388 (2020), DOI: 10.24425/aee.2020.133032

[2] Gu W., Lou G., Tan W., Yuan X., *A nonlinear state estimator-based decentralized secondary voltage control scheme for autonomous microgrids*, IEEE Transactions on Power Systems, vol. 32, no. 6, pp. 4794–4804 (2017), DOI: 10.1109/TPWRS.2017.2676181.

[3] Qian T., Liu Y., Zhang W., Tang W., Shahidehpour M., *Event-triggered updating method in centralized and distributed secondary controls for islanded microgrid restoration*, IEEE Transactions Smart Grid, vol. 11, no. 2, pp. 1387–1395 (2020), DOI: 10.1109/TSG.2019.2937366

[4] Li X., Sun Z., Tang Y., Karimi H.R., *Adaptive event-triggered consensus of multiagent systems on directed graphs*, IEEE Transactions Automatic Control, vol. 66, no. 4, pp. 1670–1685 (2021), DOI: TAC.2020.3000819.

[5] Li Z., Ren W., Liu X., Fu M., *Consensus of multi-agent systems with general linear and Lipschitz nonlinear dynamics using distributed adaptive protocols*, IEEE Transactions Automatic Control, vol. 58, no. 7, pp. 1786–1791 (2013), DOI: 10.1109/TAC.2012.2235715.

[6] Liu S., Sun J., Zhang H., Zhai M., *Fully distributed event-driven adaptive consensus of unknown linear systems*, IEEE Transactions Neural Network Learning Systems (2022), DOI: 10.1109/TNNLS.2022.3148824.

[7] Im W.S., Wang C., Liu W., Liu L., Kim J.M., *Distributed virtual inertia based control of multiple photovoltaic systems in autonomous microgrid*, IEEE/CAA Journal Automatica Sinica, vol. 4, no. 3, pp. 512–519 (2017), DOI: 10.1109/JAS.2016.7510031.

[8] Hu J., Sun Q., Wang R., Wang B., Zhai M., Zhang H., *Privacy-preserving sliding mode control for voltage restoration of AC microgrids based on output mask approach*, IEEE Transactions on Industrial Informatics, vol. 18, no. 10, pp. 6818–6827 (2022), DOI: 10.1109/TII.2022.3141428.

[9] Bidram A., Davoudi A., Lewis F.L., Guerrero J.M., *Distributed cooperative secondary control of microgrids using feedback linearization*, IEEE Transactions on Power Systems, vol. 28, no. 3, pp. 3462–3470 (2013), DOI: 10.1109/TPWRS.2013.2247071.

[10] Zhou J., Kim S., Zhang H., Sun Q., Han R., *Consensus-based distributed control for accurate reactive, harmonic, and imbalance power sharing in microgrids*, IEEE Transactions Smart Grid, vol. 9, no. 4, pp. 2453–2467 (2018), DOI: 10.1109/TSG.2016.2613143

[11] Dehkordi N.M., Sadati N., Hamzeh M., *Distributed robust finite-time secondary voltage and frequency control of islanded microgrids*, IEEE Transactions on Power Systems, vol. 32, no. 5, pp. 3648–3659 (2017), DOI: 10.1109/TPWRS.2016.2634085

[12] Ning B., Han Q.L., Ding L., *Distributed secondary control of ac microgrids with external disturbances and directed communication topologies: A full-order sliding-mode approach*, IEEE/CAA Journal Automatica Sinica, vol. 8, no. 3, pp. 554–564 (2021), DOI: 10.1109/JAS.2020.1003315

[13] Zhai M., Sun Q., Wang R., Wang B., Liu S., Zhang H., *Fully distributed fault-tolerant event-triggered control of microgrids under directed graphs*, IEEE Network Science and Engineering, vol. 9, no. 5, pp. 3570–3579 (2022), DOI: 10.1109/TNSE.2022.3176464

[14] Zhai M., Sun Q., Wang B., Liu Z., Zhang H., *Cooperative fault-estimation-based event-triggered fault-tolerant voltage restoration in islanded AC microgrids*, IEEE Transactions on Automation Science and Engineering (2022), DOI: 10.1109/TASE.2022.3186884

[15] Deng C., Che W.W., *Fault-tolerant fuzzy formation control for a class of nonlinear multiagent systems under directed and switching topology*, IEEE Transactions on Systems, Man and Cybernetics: Systems, vol. 51, no. 9, pp. 5456–5465 (2021), DOI: 10.1109/TSMC.2019.2954870.

[16] Afshari A., Karrari M., Baghaee H.R., Gharehpetian G.B., Karrari S., *Cooperative Fault-Tolerant Control of Microgrids Under Switching Communication Topology*, IEEE Transactions Smart Grid, vol. 11, no. 3, pp. 1866–1879 (2020), DOI: 10.1109/TSG.2019.2944768.

[17] Afshari A., Karrari M., Baghaee H.R., Gharehpetian G.B., *Fault-tolerant voltage/frequency synchronization in autonomous AC microgrids*, IEEE Transations on Power Systems, vol. 35, no. 5, pp. 3774–3789 (2020), DOI: 10.1109/TPWRS.2020.2975115.

[18] Zhai M., Sun Q., Wang R., Wang B., Hu J., Zhang H., *Distributed multiagent-based event-driven fault-tolerant control of islanded microgrids*, IEEE Transactions on Cybernetics (2023), DOI: 10.1109/TCYB.2023.3266923.

[19] Li X., Wen C., Chen C., Xu Q., *Adaptive resilient secondary control for microgrids with communication faults*, IEEE Transactions on Cybernetics, vol. 52, no. 8, pp. 8493–8503 (2022).

[20] Abhinav S., Schizas I.D., Ferrese F., Davoudi A., *Optimization-based AC microgrid synchronization*, IEEE Transactions on Industrial Informatics, vol. 13, no. 5, pp. 2339–2349 (2017), DOI: 10.1109/TII.2017.2702623

[21] Wang Y., Nguyen T.L., Syed M.H., Xu Y., Guillo-Sansano E., Nguyen V.H., Burt G.M., Tran Q.T., Caire R., *A distributed control scheme of microgrids in energy internet paradigm and its multisite implementation*, IEEE Transactions on Industrial Informatics, vol. 17, no. 2, pp. 1141–1153 (2021), DOI: 10.1109/TII.2020.2976830

[22] Dehkordi N.M., Baghaee H.R., Sadati N., Guerrero J.M., *Distributed noise-resilient secondary voltage and frequency control for islanded microgrids*, IEEE Transactions Smart Grid, vol. 10, no. 4, pp. 3780–3790 (2019), DOI: 10.1109/TSG.2018.2834951.

[23] Ning B., Han Q.-L., Ding L., *Distributed finite-time secondary frequency and voltage control for islanded microgrids with communication delays and switching topologies*, IEEE Transactions on Cybernetics, vol. 51, no. 8, pp. 3988–3999 (2021), DOI: 10.1109/TCYB.2020.3003690.